



# Structural, Electrical, and Magnetic Characteristics of Chemically Synthesized Lead-Free Double Perovskite: BiMgFeCeO<sub>6</sub>

Kalpana Parida<sup>1</sup> · R. N. P. Choudhary<sup>1</sup>

Received: 20 May 2020 / Accepted: 13 July 2020 / Published online: 18 July 2020  
© Springer Science+Business Media, LLC, part of Springer Nature 2020

## Abstract

In the present paper, structural, microstructural, dielectric, electrical, and magnetic characteristics of a chemically synthesized double perovskite compound BiMgFeCeO<sub>6</sub> have been reported. An analysis of room temperature X-ray diffraction data has shown formation of compound with orthorhombic symmetry. Study of micrographs of the pellets has shown the homogeneous distribution of grains, grain boundaries, and presence of required elements in the sample. Detailed studies of dielectric ( $\epsilon_r$ ,  $\tan \delta$ ) and impedance parameters of the material have provided an insight into the electrical properties and understanding of types of relaxation process occurred in the material. The semiconductor characteristic (i.e., negative temperature coefficient of resistance behavior) of the compound at high temperature has been observed in the temperature-dependent dc conductivity study. As the characteristics of the frequency dependence of ac conductivity of the material follow Jonscher's universal power law, the validity of analysis and good quality of the sample are confirmed. The occurrence of ferroelectric polarization (hysteresis loop), magnetization loop, and magnetoelectric pattern in the material confirms the multiferroicity in it.

**Keywords** Chemical reaction method · Dielectric properties · Impedance spectroscopy · Magnetic properties

## 1 Introduction

Since the discovery of ferroelectricity in barium titanate (BaTiO<sub>3</sub>), a large number of oxides of different structural family have been examined to get high dielectric constant, spontaneous polarization, piezoelectric coefficient, pyroelectric figure of merit, and low tangent loss useful for device fabrication. Among them, some lead-free (BaTiO<sub>3</sub>, BaSrTiO<sub>3</sub>) and lead-based perovskite compounds (lead zirconate titanate (PZT), lead magnesium niobate (PMN)) have been found potential for above room temperature applications and thus widely used. The lead-based perovskite ferroelectrics are toxic and volatile in nature. During high-temperature processing of lead-based compounds, the volatilization of poisonous lead oxide causes environmental pollution problem. The loss of lead also affects the electrical properties, structural instability, and composition of the materials.

Furthermore, the products having lead-based gadgets are nonrecyclable. In view of the above problems of lead compounds, now attempts are being made to develop biocompatible and environmentally friendly lead-free perovskite or double perovskite materials with enhanced ferroelectric or multi-ferroelectric properties (as compared with those of lead-based compounds) for multifunctional applications [1–3]. It is to be mentioned that double or triple perovskites give quite different structural and physical properties as compared with their constituent perovskites. Bismuth ferrite, one of the lead-free compounds, is found to have unique multifunctional applications because of its simultaneous existence of ferroelectric and antiferromagnetic ordering in a wide range of temperature (ferroelectric transition temperature  $T_C = 845$  °C and antiferromagnetic transition temperature  $T_N = 370$  °C) [4]. As compared with the other multiferroic materials, bismuth ferrite BiFeO<sub>3</sub> (BFO) has limited performance for technological applications due to its structural distortion, high leakage current, low saturation magnetization, etc. [5, 6]. To reduce or eliminate these limitations or problems, BFO is modified by appropriate substitution at its Bi/Fe sites and/or fabrication of its solid solution/composites with another similar or different structure in different ratios. The processing technique also plays an important role to synthesize phase-pure material. It has been found that lots of work have been done in the direction. Most of

✉ Kalpana Parida  
kalpanaparida0290@gmail.com

<sup>1</sup> Multifunctional Laboratory, Physics Department, Siksha 'O' Anusandhan (Deemed to be University), Bhubaneswar, Odisha 751030, India

the previous work is related to sample preparation by a conventional high-temperature solid-state reaction technique. The conventional method for synthesizing this sample suffers from the multiplication problems of nonuniformity and other problems. Therefore, to get better performance of the material proposed in the present study, we have to find out another method to produce high-quality cost-effective samples. The detailed literature survey shows that the effect of simultaneous addition of different non-iso valence element (i.e.,  $(\text{Mg}^{2+}/\text{Ce}^{4+})$  at the  $(\text{Bi}^{3+}/\text{Fe}^{3+})$  site) on structural and physical properties of BFO has not been studied and reported by chemically prepared sample so far. Therefore, with an objective to tailor the structural, dielectric, electrical, and multiferroic properties of bismuth ferrite, we have been motivated to fabricate and study a double perovskite oxides of a general formula  $A'A''B'B''\text{O}_6$  ( $A' = \text{Bi}$ ,  $A'' = \text{Mg}$ ,  $B' = \text{Fe}$ , and  $B'' = \text{Ce}$  forming  $\text{BiMgFeCeO}_6 = \text{BiFeO}_3 + \text{MgCeO}_3$ ) which should provide a reasonably better performance for devices with interesting structural, dielectric, and magnetic properties.

## 2 Experimental Methods

The polycrystalline a double perovskite of a chemical formula  $\text{BiMgFeCeO}_6$  was fabricated by a chemical reaction technique using some high-purity intergradient, such as bismuth nitrate ( $\text{Bi}(\text{NO}_3)_3 \cdot 5\text{H}_2\text{O}$ ), magnesium nitrate ( $\text{Mg}(\text{NO}_3)_2 \cdot 6\text{H}_2\text{O}$ ), iron (III) nitrate nano hydrate ( $\text{Fe}(\text{NO}_3)_3 \cdot 9\text{H}_2\text{O}$ ), and ceric ammonium nitrate  $\text{Ce}(\text{NH}_4)_2(\text{NO}_3)_6$ . These chemicals were procured from M/s Loba Chem Co Pvt. Ltd., India, in proper stoichiometric ratio. The homogeneous solution of bismuth, magnesium, iron, and ceric ammonium nitrates was prepared by using deionized water. This homogeneous solution was dried for 6 h at  $120^\circ\text{C}$  and then conducted calcination and annealing at  $750^\circ\text{C}$  for 4 h. The lump obtained was subsequently ground into fine powder, and the phase formation was examined by X-ray diffraction (XRD) structural analysis. For this, the X-ray diffraction data were collected using X-ray powder diffractometer (XRPD) (D8 Advance; Bruker) at room temperature with  $\text{CuK}\alpha$  radiation ( $\lambda = 1.5405 \text{ \AA}$ ). The cylindrical discs like pellets of 10 mm diameter and 0.5 to 3 mm thickness were molded from the calcined powder. The pellets were then sintered at  $800^\circ\text{C}$  for 8 h. In order to confirm the compactness of the fabricated pellets and to study the microstructure of the compound, scanning electron microscopy (SEM) study was performed on the pellet sample. For SEM study, the gold-coated pellet sample was used. The electrical parameters of the compound (i.e., impedance, modulus, conductivity, and dielectric) were obtained from the impedance analyzer (i.e., phase sensitive meter PSM 1735, N4L) operating in the frequency range of 1 kHz to 1 MHz at different temperature. The electrical polarization (P-E hysteresis loop) was measured at room temperature by using hysteresis loop tracer of M/s Marine India. The magnetization properties of a sample were obtained with a maximum applied field of  $\pm 8 \text{ kOe}$  at room

temperature by using VSM (vibrating sample magnetometer, Lake Shore-7410). Similarly, the magnetoelectric (M-E) coupling coefficient of the sample was obtained from the magnetoelectric coupling set up of M/s Marine India.

## 3 Results and Discussion

### 3.1 Structural and Microstructural Properties

#### 3.1.1 Structural Properties

Figure 1 represents room temperature XRD pattern of calcined powder of  $\text{BiMgFeCeO}_6$  taken in a wide range of  $2\theta$ . Preliminary X-ray structural analysis through computer software “Powd Mult” [7] shows the formation of a single-phase compound ( $\text{BiMgFeCeO}_6$ ) in orthorhombic symmetry. The best agreement between calculated and observed inter-planer distance ( $d$ ) and  $2\theta$  confirmed the above conclusion about crystal structure and symmetry (orthorhombic) of the compound. The comparison of two XRD patterns shows the chemically prepared sample well crystallized and free from experimental noise as compared with that of solid-state reaction prepared. Therefore, structural analysis has been conducted with that of chemically prepared sample. The least-squares refined unit cell parameters are  $a = 6.3409 (9) \text{ \AA}$ ,  $b = 6.4559 (9) \text{ \AA}$ ,  $c = 28.3391 (9) \text{ \AA}$ , and  $V = 1160.10 \text{ \AA}^3$  (with estimated standard deviation in the parenthesis). The normalized ( $n$ ) unit cell dimension are  $a_n = a$ ,  $b_n = b$ , and  $c_n = c/4 = 7.0848 \text{ \AA}$  which are very much consistent with those of some distorted double perovskite. The sharpness or broadening of diffraction peaks is strongly dependent on various factors including crystallite size, temperature, strain, and diffraction angles. The crystallite size ( $D$ ) of the compound has broadly been calculated putting the broadening ( $\beta$ ) of the reflection peak at half height, wavelength of the radiation used ( $1.5406 \text{ \AA}$ ), a constant  $K = 0.89$ , and Bragg angle in Scherrer equation ( $D =$

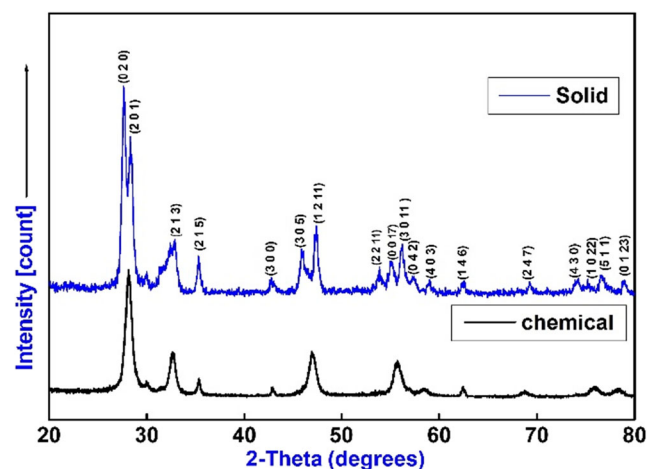
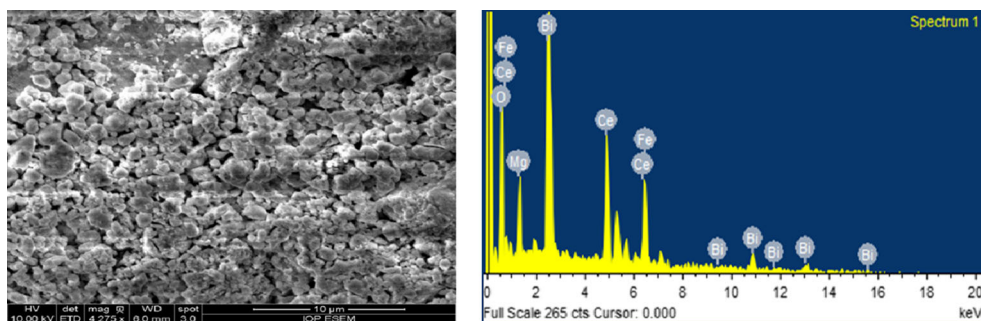
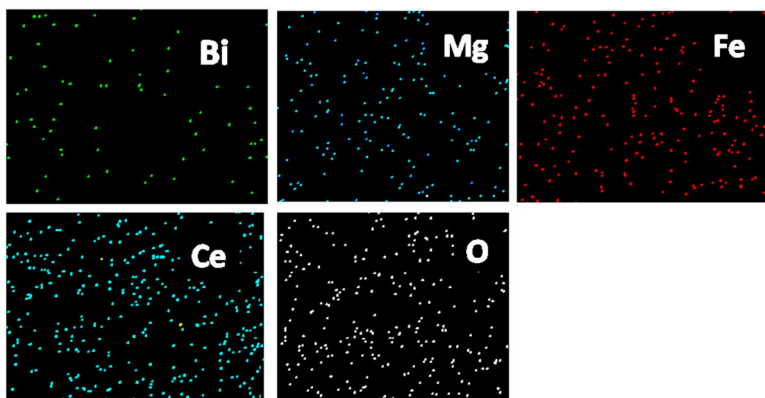


Fig. 1 Comparison of XRD pattern of  $\text{BiMgFeCeO}_6$  of solid-state reaction and chemically prepared sample

**Fig. 2** **a** SEM micrograph and **b** the energy dispersive X-ray (EDX) pattern. **c** Element mapping of chemically prepared  $\text{BiMgFeCeO}_6$



**(a)** SEM micrograph and **(b)** the energy dispersive X-ray (EDX) pattern



**(c)** : Element mapping of chemically prepared  $\text{BiMgFeCeO}_6$

$K\lambda/\beta\cos\theta$  [8] of the solid-state and chemically synthesized sample [8]. The average crystallite size of solid-state and chemically synthesized sample was found to be 24 nm and 12 nm, respectively.

### 3.1.2 Microstructural Characteristics of $\text{BiMgFeCeO}_6$

Figure 2a shows the scanning electron micrograph of  $\text{BiMgFeCeO}_6$  pellet sample. The uniform distribution of grains with different shape and size can be seen in the micrograph. In addition, presence of small voids can also be

observed. The average grain size was found to be in the range of 0.5–1.64  $\mu\text{m}$ . In comparison with the conventional solid-state method, the grain size in samples fabricated in chemical reaction route is reduced in size and closely packed [8]. Figure 2b shows the energy dispersive X-ray (EDX) pattern which reveals the presence of the elements Bi, Mg, Fe, Ce, and O in the compound. This confirms the formation of the desired compound. Figure 2c shows elementary mapping images of elements Bi, Mg, Fe, Ce, and O present in the samples. Agglomeration of elements was not observed which indicates the nonexistence of larger impurity grains [9]. From the above

**Fig. 3** **a**  $\epsilon_r$  vs frequency and **b**  $\tan\delta$  vs frequency plot for  $\text{BiMgFeCeO}_6$  at different temperatures

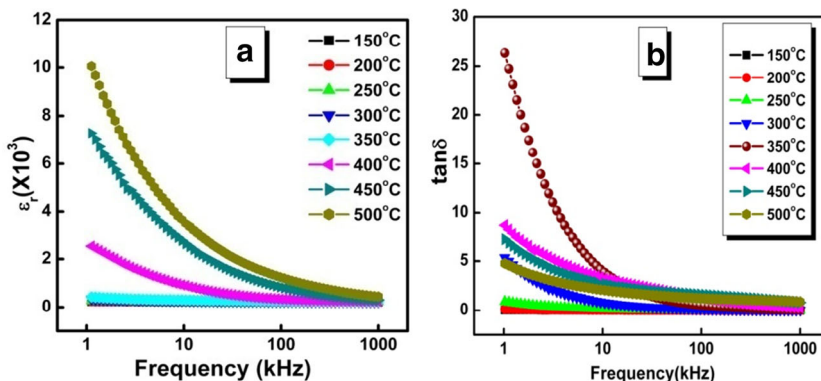
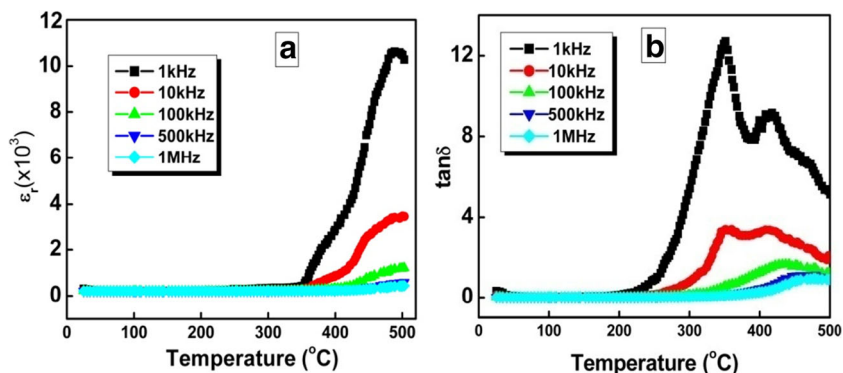


**Fig. 4** a Relative dielectric constant ( $\epsilon_r$ ) vs temperature and b loss tangent ( $\tan \delta$ ) vs temperature plot for BiMgFeCeO<sub>6</sub> at different frequencies



“**results and discussion**,” it is clear that the crystallite size ( $D$ ) of the studied material synthesized by the solid-state reaction method and the chemical reaction technique is 24 nm and 12 nm, respectively. The crystallite size is reduced by synthesizing the material by a chemical as compared with that of the conventional solid state reaction method. The grain size is found to be in the range of 0.5–2.7  $\mu\text{m}$  in solid-state method, whereas it is 0.5–1.64  $\mu\text{m}$  of the chemical method. Thus, the grain size of the sample fabricated by the chemical route is smaller and closely packed. It is observed that the synthesis process and substitution of alkaline earth metals strongly affect the grain size of the sample.

### 3.2 Dielectric Characteristics

#### 3.2.1 Frequency Dependence of Dielectric Characteristics

Figure 3 depicts the frequency dependence of relative dielectric or permittivity ( $\epsilon_r$ ) and tangent loss ( $\tan \delta$ ) up to 500  $^{\circ}\text{C}$ . With increase of frequency, the value of dielectric permittivity (Fig. 3a) and tangent loss (Fig. 3b) normally decreases and reaches at a stable point above some frequency which confirms the nature of the polar dielectrics. The high value of dielectric constant at low frequency is due to the presence of grain boundary effect, interfacial dislocations, vacancy of oxygen, etc. in the ceramic sample. A decrease of dielectric permittivity with increase in frequency generally suggests polarization based on domain switching [10].

#### 3.2.2 Temperature Dependence of Dielectric Characteristics

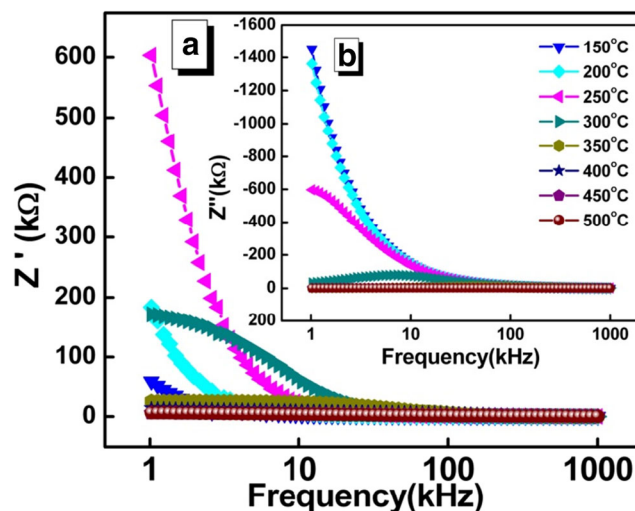
Figure 4 shows the dielectric constant vs temperature and dielectric loss vs temperature plots. In the graph, it has been observed that  $\epsilon_r$  value is almost constant up to 250  $^{\circ}\text{C}$ , and after that, it increases rapidly up to 500  $^{\circ}\text{C}$ . The value of tangent loss is low at the low temperatures, and then, it increases gradually in the high-temperature region, and it is due to the existence of few unknown defects with oxygen vacancies, impurity phases, and scattering of thermally activated charge carriers [11, 12]. A tangent loss peak-like structure

appears at 380  $^{\circ}\text{C}$  and 340  $^{\circ}\text{C}$ . With increase in frequency, the loss peak shifts to the high-temperature side. The  $\tan \delta$  value of the studied compound is found to be very small and thus has the potentiality for application in electrical devices. The relative dielectric constant of BiMgFeCeO<sub>6</sub> is larger ( $\epsilon_r = 12 \times 10^3$  at temperature 400  $^{\circ}\text{C}$  and frequency 1 kHz,) in solid-state reaction method prepared sample as compared with that of the chemically synthesized sample ( $\epsilon_r = 3 \times 10^3$  at the same temperature and frequency). It is useful to have the  $\tan \delta$  value of compound very small from both the synthesis processes ( $\tan \delta = 0.76$  at 400  $^{\circ}\text{C}$ , frequency 1 MHz) and have the potentiality for application in electrical devices. The higher value of the dielectric compounds BiMgFeCeO<sub>6</sub> prepared by solid-state reaction method is due to the existence of few unknown defects with oxygen vacancies, impurity phases, etc.

### 3.3 Impedance and Modulus Spectroscopy Study

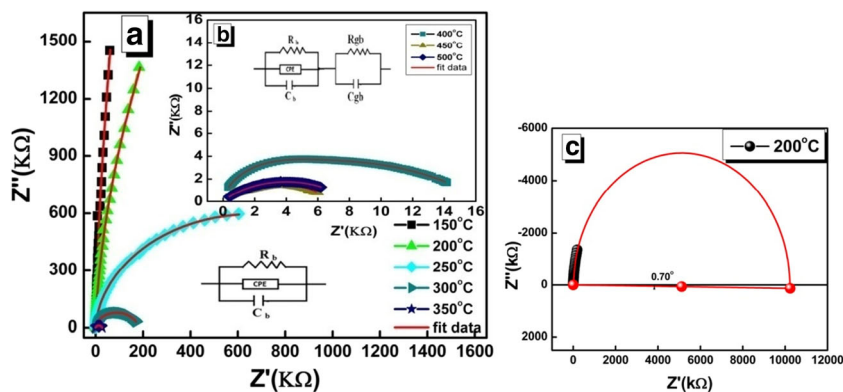
#### 3.3.1 Impedance Studies

Figure 5 depicts the variation of real ( $Z'$ ) and imaginary ( $Z''$ ) components of impedance at selected temperatures for



**Fig. 5** a Frequency variation of  $Z'$ , b (insert) frequency variation of  $Z''$  at selected temperatures of BiMgFeCeO<sub>6</sub>

**Fig. 6** Variation of  $Z''$  with  $Z'$  at **a** 150–350 °C, **b** 400–500 °C, and **c** depression angle at 200 °C for  $\text{BiMgFeCeO}_6$



$\text{BiMgFeCeO}_6$  ceramic samples. It is observed in the graphs that the value of  $Z'$  increases with increase in temperature up to 250 °C, and thereafter, it decreases with increase in temperature. This feature is at variance with the other alkaline earth metal oxides, wherein semiconductor nature (as suggested by negative temperature of coefficient of resistance (NTCR) behavior of graphs) of the material at high temperature was reported for the entire frequency range [13]. At high frequency, the values of  $Z'$  converge for all the studied temperatures, suggesting release of space charge [14] in the  $Z''$  vs frequency curve. A relaxation peak [15] is observed at high temperatures. There is a tendency of a peak formation below the experimental value of 1 kHz in the sample prepared through chemical route.

Figure 6 exhibits the Nyquist ( $Z''$  vs  $Z'$ ) plots for the  $\text{BiMgFeCeO}_6$  sample. The equivalent circuit obtained on the basis of the data analyzed with the use of Zsimp win software is inserted in each of the figures. The values of grain boundary resistance ( $R_{gb}$ ), grain resistance ( $R_b$ ), grain boundary capacitance ( $C_{gb}$ ), and bulk capacitance ( $C_b$ ) were listed in Table 1. It is observed that the grain boundary effect is found to

activate at the temperatures above 350 °C. The electrode effect is not observed in the experimental temperature limit of 500 °C. The depression angle of the semicircular arc, which is an estimate of the deviation from the ideal Debye-type relaxation behavior, is found to be 0.7° (Fig. 6c) at 200 °C of the studied sample. The magnitude of real part of impedance ( $Z'$ ) of  $\text{BiMgFeCeO}_6$  prepared by solid-state method at 1 kHz is 400 k $\Omega$ , whereas by chemically prepared sample, it is 600 k $\Omega$  which is much higher than that of to the sample prepared by the solid-state reaction method.

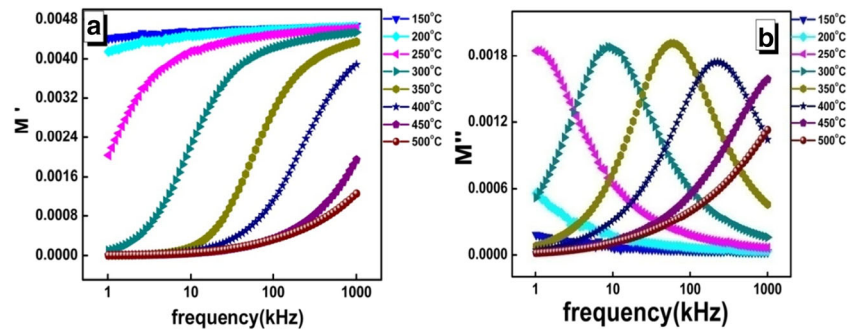
### 3.3.2 Modulus Analysis

Figure 7a represents the changes of  $M'$  (real part) with frequency at selected temperature of the studied temperature range (150–500 °C). For all the temperatures, the value of  $M'$  increases with increase in frequency and tends to attain a constant value at high frequencies. Such type of tendency indicates that with increase in frequency, each ion atom travels over a shorter distance in the electric field until the electric

**Table 1** Calculated value of  $R_b$ ,  $R_{gb}$ ,  $C_b$ , and  $C_{gb}$  of  $\text{BiMgFeCeO}_6$  at selected temperatures

Temp. (°C)	Model	$R_b$ ( $\Omega$ )	$C_g$ (farad)	$R_{gb}$ ( $\Omega$ )	$C_{gb}$ (farad)
150	(RQC)	8.568E+007	1.003E-010	–	–
200	(RQC)	1.757E+007	1.007E-010	–	–
250	(RQC)	1.393E+006	1.006E-010	–	–
300	(RQC)	1.874E+005	1.009E-010	–	–
350	(RQC)	2.714E+004	9.667E-011	–	–
400	(RQC) (RC)	1.352E+004	1.501E-010	3.052E+003	2.556E-010
450	(RQC) (RC)	6.560E+003	4.634E-009	4.281E+002	4.628E-010
500	(RQC) (RC)	8.063E+003	2.778E-007	1.000E-002	2.514E-014

**Fig. 7** **a**  $M'$  vs frequency and **b**  $M''$  vs frequency for BiMgFeCeO<sub>6</sub> at different temperatures

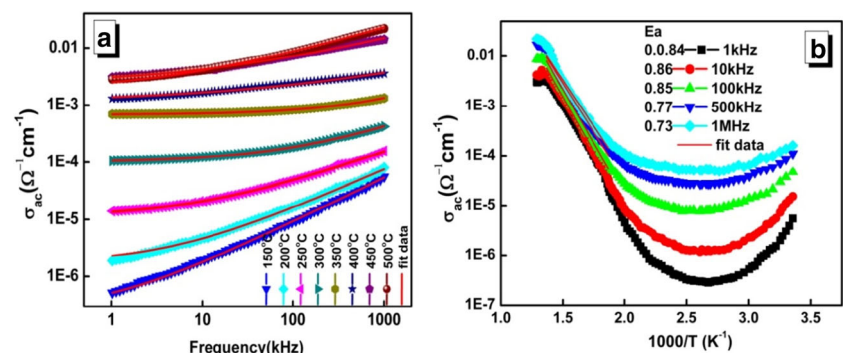


field changes so speedily that the ions only rattle within the confinement of their potential energy wells. The change of  $M''$  with frequency at various temperatures is presented in Fig. 7b.

### 3.4 Conductivity Analysis

Figure 8a depicts the variation of  $\sigma_{ac}$  with frequency at a set of temperature of the tested sample. As can be seen in the figure for high temperature (i.e., above 400 °C), the conductivity is almost independent of frequency implying the dominance of dc conductivity at these temperatures. The variation of  $\sigma_{ac}$  with frequency obeys the universal Jonscher power law:  $\sigma_1 = \sigma_{dc} + B\omega^n$ . In Fig. 8a, it can be observed that with the increase in temperature, the frequency corresponding to prominent dispersion of  $\sigma_{ac}$  moves towards the low frequency side [16]. The variation of  $\sigma_{ac}$  conductivity of BiMgFeCeO<sub>6</sub> with  $10^3/T$  at different frequencies is given in Fig. 8b. At low temperatures, an increase in the ac conductivity with the increase in frequency can be observed. This indicates the dispersion of conductivity with frequency. However, with the increase in frequency, the change in ac conductivity reduces. On the other hand, at high temperatures, all the curves at various frequencies tend to merge, and dispersion in conductivity narrows down with increase in temperature. This implies that the conductivity enters a zone where it is almost frequency independent (i.e., the dc conductivity becomes dominant) [17, 18]. The NTCR behavior can be understood from the increase in conductivity of the material with increase in temperature. The values of activation energy ( $E_a$ ) at high temperatures (300–500 °C) are high as compared with that of low temperature. The  $E_a$  values calculated at different frequencies are provided in the figure.

**Fig. 8** Variation of ac conductivity with **a** frequency at different temperatures and **b** inverse of absolute temperature at different frequencies



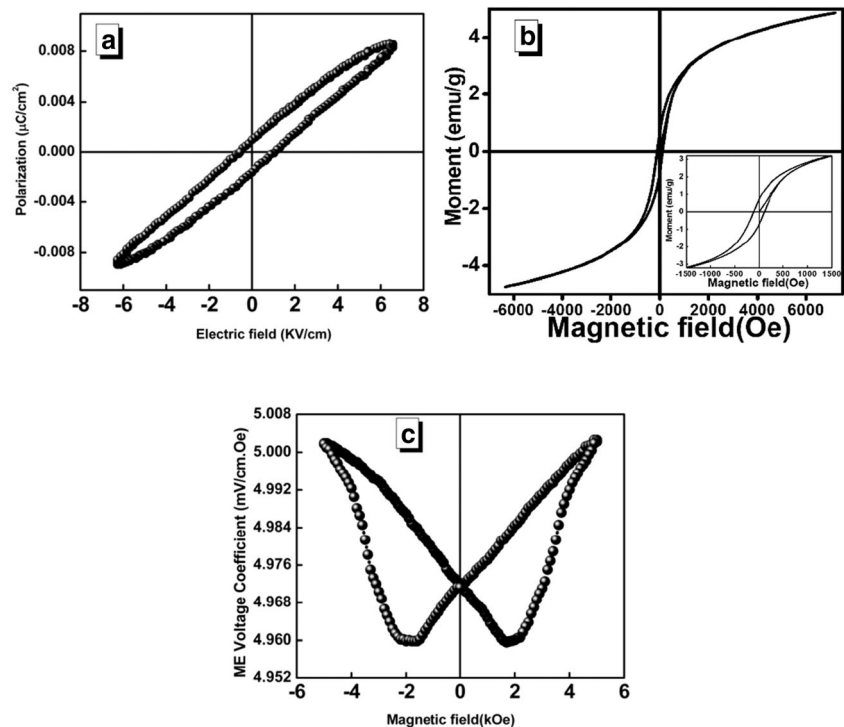
### 3.5 Multiferroic Properties

The appearance of P-E hysteresis loop measured at room temperature of BiMgFeCeO<sub>6</sub>, shown in Fig. 9a, confirms the ferroelectric nature of the sample. Figure 9b depicts the magnetic hysteresis loop of the compound which was recorded by applying magnetic field of about  $\pm 8$  kOe at the room temperature. The characteristics of the hysteresis loop suggest the existence of ferromagnetic nature of the study material.

Generally, bismuth ferrite has G-type of magnetic structure with antiferromagnetic behavior, where antiferromagnetic coupling between adjacent planes and ferromagnetic coupling of the magnetic moment of Fe<sup>3+</sup> cations in pseudo-cubic planes occur. The value of magnetic parameters is obtained using magnetic field dependent magnetization (M-H) loop. The loop parameters obtained for the study material are remnant magnetization ( $M_r$ ) = 0.08 emu, saturation magnetization ( $M_s$ ) = 4.8 emu/g, and coercivity ( $H_c$ ) = 114 Oe. It has been seen that the above M-H loop parameters of the Mg/Ce modified bismuth ferrite double perovskite BiMgFeCeO<sub>6</sub> show its enhanced magnetic properties as compared with those of the parent BFO compound.

The ME coefficient  $\alpha_{ME}$  of the multiferroics material is measured after poling the sample both electrically and magnetically to maximize the interaction between the sublattices which leads to maximum ME effect [19, 20]. In the present work, the zero field  $\alpha_{ME}$  value is found to be 5.0 mv/cm Oe. It is an established fact that the strong ME effect is due to the great interfacial and good phase connectivity. Here, the fillers are ferrite nanoparticles with no agglomeration, as confirmed

**Fig. 9** **a** P-E hysteresis loop, **b** M-H hysteresis loop, and **c** variation of ME voltage coefficient with applied magnetic field at room temperature of BiMgFeCeO<sub>6</sub>



from the SEM micrograph. These particles have large interfacial area favoring the elastic interaction between the ferromagnetic and ferroelectric phase and result in strong ME effect. The magnitude of the ME coefficient of BiMgFeCeO<sub>6</sub> of the solid-state reaction method prepared sample is 2.664 mV/cm Oe, whereas it is 5.006 mV/cm Oe for chemically prepared sample. Thus, ME coefficient value is larger in chemical reaction synthesis process as compared with that of solid-state reaction method [8].

## 4 Conclusion

The detailed analysis of X-ray diffraction data and microstructural images of chemically prepared BiMgFeCeO<sub>6</sub> have shown that prepared compound is a single-phase material with uniformly distributed grains across the entire surface and absence of foreign elements. The temperature and frequency significantly affect the dielectric parameters of the compound. Both bulk material and grain boundary effect are responsible for the conduction properties of the compound, as found from the impedance spectra analyses. At low frequencies and high temperatures, the role of grains and grain boundaries in conduction process is well explained by Maxwell-Wagner mechanism. The P-E hysteresis, M-H hysteresis loop, and M-E coupling coefficient confirm the multiferroic nature of BiMgFeCeO<sub>6</sub>. From the above observations, it can be suggested that this material can have some possible applications in sensors; data storage recorder; and random-access multi-

state memories, absorber, transducers, spintronic, etc. Finally, it is concluded that the chemically synthesized material provides homogeneous and highly compact grain morphology. As a result, we obtain stable structure with enhanced mechanical and electric transport characteristics of the material.

**Acknowledgments** The authors are grateful to Dr. Satyabati Das, Indian Institute of Technology, Bhubaneswar, India, and Professor. Perumal Alagarsamy, I I T Guwahati, Assam, India, for their kind help in some experimental work.

## References

1. Ringgaard, E., Wurlitzer, T.: *J. Eur. Ceram. Soc.* **25**, 2701 (2005)
2. Maeder, M.D., Damjanovic, D., Setter, N.: *J. Electro. Ceram.* **13**, 385 (2004)
3. Wolny, W.W.: *Ceram. Int.* **30**, 1079 (2004)
4. Polomska, M., Kaczmarek, W., Pajak, Z.: *Phys. Status Solidi.* **23**, 567 (1974)
5. Das, R., Khan, G.G., Mandal, K.: *J. Appl. Phys.* **111**, 104 (2012)
6. Lan, C., Jiang, Y., Yang, S.: *J. Mater. Sci.* **46**, 734 (2011)
7. POWDMULT: an interactive powder diffraction data interpretation and indexing program version 2.1, E. Wu, School of Physical Sciences, Flinders University of South Australia, Bradford Park, SA 5042, Australia
8. Parida, K., Dehury, S.K., Choudhary, R.N.P.: *Phys. Lett. A.* **380**, 4083 (2016)
9. Begum, H.A., Naganuma, H., Oogane, M., Ando, Y.: *Materials.* **4**, 1087 (2011). <https://doi.org/10.3390/ma4061087>
10. Pradhan, D.K., Choudhary, R.N.P., Rinaldi, C., Katiyar, R.S.: *J. Appl. Phys.* **106**, 024102 (2009). <https://doi.org/10.1063/1.3158121>

11. Pawar, R.P., Puri, V.: *Ceram. Int.* **40**, 10423 (2014)
12. Sen, S., Choudhary, R.N.P.: *Mater. Chem. Phys.* **87**, 256 (2004)
13. James, A.R., Prakash, C., Prasad, G.: *J. Phys. D. Appl. Phys.* **39**, 1635 (2006)
14. Suman, C.K., Prasad, K., Choudhary, R.N.P.: *J. Mater. Sci.* **41**, 369 (2006)
15. Chatterjee, S., Mahapatra, P.K., Choudhary, R.N.P., Thakur, A.K.: *Phys. Status Solidi.* **201**, 588 (2004)
16. Hirose, N., West, A.R.: *J. Am. Ceram. Soc.* **79**, 1633 (1996)
17. Mishra, S.N., Choudhary, S.N., Choudhary, R.N.P., Murthy, V.R.K., Prasad, K.: *J. Mater. Sci. Mater. Electron.* **23**, 185 (2012)
18. Gabal, M.A.E.F., Al Angari, Y.M., Obaid, A.Y.: *C. R. Chim.* **16**, 704 (2013)
19. Pahuja, P., Prakash, C., Tandon, R.P.: *Ceram. Int.* **40**, 5731 (2014)
20. Parida, K., Dehury, S.K., Choudhary, R.N.P.: *J. Mater. Sci. Mater. Electron.* **27**, 11211 (2016)

**Publisher's note** Springer Nature remains neutral with regard to jurisdictional claims in published maps and institutional affiliations.